Using spatial patterns of fluvial incision to constrain continental-scale uplift in the Andes.

L.A. Evenstar*[1], A.E. Mather[2] and A.J. Hartley[3]

[1]School of Environment and Technology, University of Brighton, UK,

[2]Department of Geography, Earth and Environmental Sciences, University of Plymouth, UK,

[3]Department of Geology and Petroleum Geology, University of Aberdeen, Aberdeen, UK,

Abstract

Geomorphic archives, particularly longitudinal river profiles, are increasingly used as a proxy to reconstruct uplift rates in mountainous regions. Within the Atacama Desert, Northern Chile, slow, long-term erosion creates exceptional preservation of fluvial and alluvial surfaces. This enables river incision patterns to be used on a continental-scale (>250 km) along the western margin of the Andes (18°00'S to 20°15'S) and over a time frame from Miocene to Present day. The data show marked compartmentalisation of fluvial system behaviour with changes in incision rates from south to north creating 3 distinctly different regions. Within these different sectors, incision rates are broadly consistent between rivers suggesting a regional rather than a river specific control on rates. In Sector 1 (18°05'S to 19°20'S) the fluvial systems are exorheic with a terminal base level (the lowest base level to which the river system can erode) in the Pacific Ocean and span the Coastal Cordillera, Longitudinal Valley, Precordillera and western edge of the Western Cordillera. This constrains the total uplift over these regions to a minimum of 1200 m in 11 Myr with incision rates of ~200-120 m/Myr consistent with rapid but sustained uplift of the Andes in the Late Miocene. In Sector 2 (19°20'S to 19°50'S), to the immediate south, the rivers are shorter and terminate in the Longitudinal Valley, spanning only the Longitudinal Valley, Precordillera and the western edge of the Western Cordillera with lower incision rates of 100-50 m/Myr. Comparison of incision rates between Sector 1 and 2 can constrain the uplift of the Coastal Cordillera to 60m/Myr which is in keeping with previous studies from the region. In southernmost Sector 3 (19°50'S to 20°10'S), the fluvial systems terminate in the Longitudinal Valley and span only the Longitudinal Valley and eastern part of the Precordillera with low incision rates of 50 to 25 m/Myr.

Differences between Sectors 2 and 3 are attributable to drainage loss by tectonic
beheading of catchments through uplift of the Cordillera de Domeyko fault system,
placing a minimum constrain on uplift in this region of 50 to 25 m/Myr. This study
demonstrates the applicability of large-scale fluvial archives to access not just the
timing of uplift on a continental scale, but also the relative uplift of individual tectonic
provinces.

Keywords; Andes; Paleosurface; Atacama; Desert Pavement; landscape evolution;
climate; base levels; fluvial incision, fluvial archives, terraces.

1. Introduction

Fluvial geomorphological archives are being increasingly used to reconstruct climate
and deformation (e.g. Macklin et al., 2002, Bridgeland et al., 2012, Stokes et al.
2017, Evenstar et al. 2018; Stokes et al., 2018). These archives comprise dominantly
erosional (e.g strath terrace) through to depositional records (e.g. distributive fluvial
systems) and can be regionally extensive (e.g. pediment systems). The common
theme is that these types of geomorphic archive have low angle surface expressions
which can be reconstructed to enable surface deformation to be quantified (e.g.
Gesch et al., 2014; Demoulin et al 2017, Stokes et al., 2018). Typically the majority of
these studies concentrate on a single pediment surface over small basin scale or
focus on trunk drainage or tributaries along a single river system (e.g. Anton et al.,
2014, Martins et al., 2017, Evenstar et al., 2018). Whilst correlation of fluvial system
behaviour has been attempted across regional scales (>100's km) to examine
climate controls (e.g. Macklin et al, 2002), flooding records (e.g. Benito et al., 2000)
and uplift rates (Litchfield and Berryman 2006) this has typically been restricted to
time-scales younger than the Pliocene. The few studies that look at regional scale
deformation over longer timescales tend to utilise modelling of profiles or terrace
patterns due to limited preservation of the fluvial system (e.g. Demoulin et al., 2007,
Boulton et al., 2014). Where appropriate records are well preserved (e.g. in arid
landscapes), availability of high-resolution satellite data sets facilitate regional
geomorphic reconstruction over much wider spatial and temporal scales than was
previously possible.

The Atacama is the most arid and potentially, oldest desert region in the world
(Hartley et al., 2005, Dunai et al., 2005). The long term sustained arid climate leads
to preservation of ancient landscapes, some of which are dated back to the Late

74 Oligocene (Dunai et al. 2005, Evenstar et al. 2009, Evenstar et al. 2017). Several of

75 these surfaces are identified as being generated following abandonment of fluvial

76 incision events associated with fluctuating climate and long-term uplift of the Andean

77 mountain chain (Evenstar at al. 2017). Within hyper-arid fluvial systems, as a function

78 of their low geomorphic erosional efficiency, even modest vertical crustal uplift is

79 likely to be more directly expressed as surface uplift, and thus more likely to be

80 recorded within fluvial archives (e.g. Demoulin et al., 2017). In the central Andes

81 (Atacama Desert) the sustained dominance of extreme aridity is expressed by the

82 presence of near linear to convex hypsometric curves that are typical of areas

83 experiencing ineffective fluvial incision (Montgomery et al., 2002). This incision, in

84 response to tectonic uplift, is documented in the fluvial archives, and along with the

85 past climate (e.g. Dunai et al., 2005; Evenstar et al., 2009; Evenstar et al., 2017),

86 these fluvial archives are increasingly well understood (Victor et al., 2004, Farías et

87 al., 2005, Jordan et al., 2014, van Zalinge et al., 2017) and can be exploited to

88 examine continental scale uplift. These approaches have documented vastly different

89 rates of fluvial incision in northern Chile from 100 m/m.y. (Hoke et al., 2007) to 10

90 m/m.y (Cooper et al., 2016) since the Middle Miocene leading to different models for

91 timing of Andean uplift.

92

93 Here, we utilise freely available satellite remotely sensed data, together with longer

94 term geological and geomorphological erosional and depositional records to

95 reconstruct and quantify the last 11 Myr of pediment and fluvial landscape erosion

96 along the western side of the Central Andes orogen, a classic subduction zone

97 setting. The low erosional efficiency of this landscape means that the surface uplift is

98 preserved in excellent detail. The present study seeks to establish a continental scale

99 view of the fluvial incision and how this varies parallel to the Andean Mountain chain.

100 Using this we aim to establish the main controlling factors on incision rates in order to

101 better understand their use in constraining continental scale uplift within the Central

102 Andes.

103

104 **2. Study area: landscape components and depositional record**

105 The study region runs along the western margin of the Central Andean mountain

106 range from 18°00'S to 20°15'S (Figure 1a). This region consists of several different

107 morphotectonic provinces; the Coastal Cordillera, Longitudinal Valley, Precordillera

108 and Western Cordillera (Figure 1a). The Coastal Cordillera runs along the coast of

109 the Pacific Ocean and is characterised by the eroded Jurassic magmatic arc. The

110 Coastal Cordillera is absent around the border between Chile and Peru (18°30'S) but

111 increases in width and height towards the south (Madella et al., 2017). The Coastal
112 Cordillera shows exhumation back to the Eocene (Juez-Larre et al., 2010). However
113 the timing of uplift of this range is poorly constrained with rates varying from
114 0.001mm/yr to 0.1 mm/yr proximal to the coast (Regard et al. 2010; Garcia-Perez et
115 al., 2018) to 0.05 mm/yr to 0.07 mm/yr inland (Hartley et al., 2000; Dunai et al., 2005;
116 Cosentino and Jordan 2017). On the regional scale the mountain range was still at or
117 close to sea level in the Late Oligocene forming the regionally extensive Tarapaca
118 surface that graded down to sea level (Noble et al., 1985, Delouis et al., 1998, Dunai
119 et al., 2005; Thouret et al., 2007). The mountain range is believed to have uplifted
120 continuously from the late Oligocene at an average rate of 0.05 mm/yr to 0.07 mm/yr
121 (Delouis et al., 1998; Hartley et al., 2000; Dunai et al., 2005; Cosentino and Jordan
122 2017). To the east, the Coastal Cordillera borders the Longitudinal Valley, a deep
123 fore arc basin infilled with Oligocene to Miocene aged sediments derived from the
124 Andean mountain range to the east (Evenstar et al., 2009; Hartley & Evenstar 2010).
125 The top of the basin is characterized by an elevated low-relief relict landscape
126 termed the Pacific Paleosurface (PPS) (Evenstar et al., 2017). The Longitudinal
127 Valley is characterized by a series of westward propagating reverse faults or
128 monocline folds which have been active from ~30 to 5 Ma (Victor et al., 2004, Garcia
129 2005, Farías et al., 2004). To the east of the Longitudinal Valley lies the
130 Precordillera. This rises in elevation from 2000 to 4000 masl and is characterized by
131 a series of westward propagating, north-south striking thrusts and folds related to the
132 Domeyko fault system (Figure 1). The Precordillera forms the foothills to the modern
133 magmatic arc in the east, termed the Western Cordillera with peaks up to 6000 m.
134
135 The Precordillera and Longitudinal Valley are infilled by volcaniclastic and fluvial
136 sediments, which were predominantly deposited syn-tectonially (Figure 2). The oldest
137 sediments in the region are the Azapa Formation, a series of alluvial conglomerates
138 dated at ~35 to 22.7 Ma (Wörner et al., 2000; Wotzlaw et al., 2011; van Zalinge et.,
139 2017). Overlying the Azapa Formation in the Longitudinal Valley, and unconformably
140 overlying the basement in the Precordillera, are a series of ignimbrites and
141 volcaniclastic sediments termed the Oxaya Formation (22.7 Ma -19.7 Ma) (Wörner et
142 al., 2000; van Zalinge et., 2017). North of 19°00'S, these deposits are predominantly
143 formed by thick ignimbrite sheets (up to 1000 m) (van Zalinge et al., 2017). In the
144 area around the Lluta Quebrada, the ignimbrite sequence forms the top of the
145 stratigraphic succession in the Longitudinal Valley (Figure 2 and 3). In contrast,
146 towards the south, the ignimbrite sheets thin and are intercalated with more fluvial
147 sediments (Hartley and Evenstar, 2010). South of Quebrada Lluta, the volcaniclastic

148   sediments in the Longitudinal Valley are conformably overlain by the El Diablo

149   Formation (Figure 2), a series of fluvial sediments dated at 16 -11 Ma (Evenstar et

150   al., 2017). Within this region the El Diablo Formation is overlain by the Tana lava

151   dated at 8.8 ± 0.5 Ma (Mortimer et al., 1974) and 8.2 ± 0.5 Ma (Muñoz and

152   Sepulveda, 1992) constraining the age of the end of the El Diablo Formation to 11-8

153   Ma.

154

155   This study focuses on the PPS which is formed from numerous distributive fluvial

156   systems, which can be found in the Longitudinal Valley and in parts of the

157   Precordillera (Evenstar et al., 2017). North of 19°20'S, the PPS is deeply dissected

158   (up to 1,700 masl) by five main rivers (Lluta, Azapa, Victor, Camarones and Tana)

159   that drain to the Pacific Ocean (exorheicly drained) with a terminal base level of 0

160   masl (Fig. 1). Analysis of the fluvial profiles of Quebrada Tana shows that the main

161   knickpoint is within the Coastal Cordillera (Garcia et al., 2011; Evenstar et al., 2017;

162   Kirk-Lawlor et al., 2013), suggesting that it has not yet adapted to the new terminal (0

163   masl) base level, with the upper reaches of the river still grading down to the former

164   terminal base level within the Longitudinal Valley at 1000 masl (Kirk-Lawlor et al.,

165   2013; Evenstar et al., 2017). The timing of when fluvial regions north of Quebrada

166   Tana became exorheicly drained is considered to be diachronous from the Early to

167   Mid Miocene (Evenstar et al., 2017). South of this region, the main rivers (Aroma,

168   Tarapaca, de Parca and Tambillo) terminate within the Longitudinal Valley

169   (endorheicly drained) with terminal base levels of ~1000 masl and incise the PPS

170   towards the Western Cordillera by up to 1000 masl (Hoke et al., 2007).

171

172   The PPS can be traced for over 600 km (south to north) within the Longitudinal

173   Valley. The surface has been mapped in detail using remote sensing techniques and

174   constrained in age using cosmogenic isotope dating techniques in Evenstar et al.,

175   (2017). This research demonstrates that the PPS is in fact formed from an

176   amalgamation of geomorphic surfaces (both erosional (inset) and depositional

177   (overlying)) spanning a range of ages from the Late Oligocene to present day

178   (Evenstar et al., 2009; 2017). The timing of formation of the surface is related to

179   regional climate while the geographical location of the individual components that

180   comprise the surface are controlled by regional tectonic activity (Evenstar et al.,

181   2017). Within the present study we examine the youngest three geomorphic

182   surfaces; Aggradational Surface 4 (AS4), Degradational Surface 3 (DS3) and

183   Degradational Surface 2 (DS2) (Terminology after Evenstar et al., 2017 and shown in

184   Figure 2 and 3). Aggradational surface 4 (AS4) represents the end of deposition of

185 the El Diablo formation and is dated at 11 Ma using *insitu* exposure ages (Evenstar

186 et al., 2017). Degradational surface 3 (DS3) is an erosion system which cuts into the

187 underlying sediment fill of the basin (El Diablo Formation and Oxaya Formation). The

188 surface comprises a relict dendritic drainage pattern abandoned at ~7 Ma (*insitu*

189 exposure ages, Evenstar et al., 2017). Degradational System 2 (DS2) cuts into the

190 older geomorphic surface DS3 and is characterized by a trellis drainage pattern. The

191 abandonment of this surface is constrained at ~3 Ma (Evenstar et al., 2017). Along

192 the Quebrada Lluta, lies a large (26 km^3) landslip deposit, the Lluta collapse, which

193 disrupts various surfaces. This feature shows westward collapse into the Longitudinal

194 Valley and is believed to have formed at ~3 Ma (Wörner et al., 2002: Kober et al.,

195 2007; Evenstar et al., 2017).

196

197 The timing and rate of uplift of the Andes is still ambiguous, with two favoured end-

198 member models (Fig. 2); (1) rapid, late Miocene uplift, with surface uplift of ~2.5 km

199 between 11 and 6 Ma (e.g. Garzione et al., 2006; Ghosh et al., 2006, Garzione et al.,

200 2008); and (2) slow and steady uplift that started in the late Eocene (e.g. Victor et al.,

201 2004; Hartley et al., 2007; Barnes and Ehlers, 2009; Evenstar et al., 2015; van

202 Zalinge et al., 2017). Thus, the eastern edge of the PSS has experienced substantial

203 cumulative surface uplift regardless of which model is taken throughout the Miocene

204 and Pliocene. Several studies have used the main fluvial systems in the region to

205 calculate regional uplift of the Andes across the region (e.g. Farías et al., 2005, Hoke

206 et al., 2007; Schildgen et al., 2002; Schildgen et al., 2009). However, more recent

207 climate modelling of this region has cast doubt on this interpretation suggesting

208 higher incision rates could be due to increased orographically generated precipitation

209 (Ehlers and Poulsen, 2009).

210

211 Along the western margin of the Andes, the PPS has been undergoing uplift since at

212 least the Early Miocene (Evenstar et al., 2015) and likely extends back further to the

213 early Oligocene (Barnes and Ehler 2009, van Zalinge et al., 2017). The uplift of the

214 region is modified locally predominantly north-south fault systems (Figure 1) (Wörner

215 et al. 2002; Victor et al. 2005; Farías et al. 2005; van Zalinge et al. 2017) with minor

216 amounts of surface uplift expressed as regional tilting (Farías et al. 2005). However,

217 there are no marked changes in regional tectonic uplift from North to South over the

218 study area with similar rates and timing of uplift (2500m to 3200m of uplift during 25

219 Ma to 8 Ma) reported from 18°S to 22°S in Northernmost Chile by numerous authors

220 (Wörner et al., 2002; Victor et al., 2005; Farías et al., 2005; Jordan et al., 2014;

221 Evenstar et al., 2015; van Zalinge et al., 2017).

222

3. Study area climate

The past climate of the region is reasonably well constrained (Fig. 2). The climate has been arid to semi-arid since at least the late Jurassic (Hartley et al., 2005), arid since the late Oligocene and predominantly hyperarid since the mid Miocene (Evenstar et al., 2009, Jordan et al., 2014, Evenstar et al., 2017, Rech et al., 2019). Since the Oligocene, short intervals (< 1 myr) of slightly more humid conditions have been recorded (Evenstar et al., 2009, 2015, 2017; Jordan et al., 2014) (Fig. 2). These humid intervals are within the range of an arid climate with annual mean precipitation rates less than 100 mm/yr, below the threshold for the establishment of significant vegetation cover (Jordan et al., 2014). As a result of the long-lived regional persistent climatic aridity, the PPS is exceptionally well preserved, providing a unique opportunity to examine the development of regionally extensive paleo-fluvial surfaces in a non-vegetated regime over geologic time-scales.

4. Methodology and Approach

4.1 Reconstructing regional fluvial palaeo-surfaces.

Relict paleo-surfaces of the PPS combined with the elevation data in the Longitudinal Valley were used to identify and extrapolate geomorphic surfaces (pediments and valley bottoms) throughout the past ca. 11 Myr. Four regional elevation profiles (A-D) were constructed across the PPS, one parallel to the drainage (A-East to West) and three perpendicular to the drainage (B, C and D-North to south) (Fig. 3). The landscape profiles were constructed using DEM data from Shuttle Radar Topography Mission (SRTM) data with 30 m resolution (Figs. 3 and 4). Profile A is 45 km long and runs from east to west at 18°45'S (Fig. 3). The three other topographic profiles are 260 km long and run parallel along the eastern edge of the Longitudinal Valley from southern Peru at 18°05'S towards northern Chile at 20°15'S (Location in Figure 3 and cross sections in Figure 4). These profiles cross three of the main paleo-surfaces mapped within the regions (AS4, DS3 and DS2) (Fig. 3). On each profile the remnant parts of the various paleo-surfaces (as mapped by Evenstar et al, 2017) are highlighted (Figs.3 and 4). Using the preserved remnants of these surfaces (palaeosurface residual highs, inset terraces and valley bottom elevations) we can extrapolate the line of maximum incision levels of the main quebradas across the region (Figs.3 and 4).

259

260   Surface AS4 is formed as a series of relict distributive fluvial systems with a low

261   gradient slope and is preserved on the west edge of profile A forming a plateau (Fig.

262   3). Using the slope of AS4, the surface can be projected towards the east (Fig. 3).

263   Within profiles B-D, AS4 is preserved in the south as a series of relict inselberg

264   surfaces which can be correlated across the southern region to reconstruct the paleo

265   fluvial surface (Fig. 4). Towards the north of Quebrada Camarones, the preservation

266   of the AS4 surface decreases and the surface cannot be accurately mapped north of

267   Quebrada Lluta.

268

269   Surface DS3 formed as a tributive fluvial system incised into AS4. It is well preserved

270   within the central parts of profile A cutting into AS4 and forming a low angle erosional

271   surface. This surface can be projected to the east using the slope angle (Fig. 3).

272   Within profiles B-D, DS3 is mapped as a series of relict inselberg highs north of

273   Quebrada Lluta (Figs. 4 and 5A-B). These highs in profiles B-D can be linked across

274   the region forming a single surface down to Quebrada Camarones. South of this

275   point, where AS4 is preserved, DS3 incises into AS4 and forms a series of lower

276   terraces (Figs. 4 and 5C).

277

278   Surface DS2 is preserved along the eastern edge of Profile A cutting into DS3 and

279   forming a low angle erosional surface (Fig. 3). Within Profiles B to D, this surface

280   forms the lowest incision surface north of Quebrada Lluta that can be correlated

281   across this region (Figs. 4 and 5A-B). Towards the south, this surface is constrained

282   within the main quebradas and forms a series of terraces. The Lluta ignimbrite is

283   preserved along these terraces and has previously been used to reconstruct the relict

284   river profiles at 2.7 Ma along the Quebrada Lluta which can be linked with this

285   surface (Kober et al. 2006).

286

287   In the southernmost part of the region the laterally traced fluvial archives are

288   correlated with the depths and timing of water table drops in the Cerro Colorado mine

289   that have been reconstructed using hematite age-dates from drill core (Cooper et al.

290   2016) (Fig. 4). Throughout the region, the present-day fluvial cross-profiles were

291   reconstructed utilising the lowermost incisional points within the modern-day

292   perennial rivers (Fig. 4).

293

294   **4.2 Palaeo-surface age constraints.**

295

296   Age constraints on the surfaces are based on previously published *insitu* exposure

297   age dating (Kober et al., 2007, Evenstar et al., 2009, Evenstar et al., 2017), dated

298   volcanics (Wörner et al., 2002, Kober et al., 2006, Hoke et al., 2007) and hematite

299   age-dates from drill core (Cooper et al., 2016). These constraints are shown where

300   they intersect the elevation profiles in Figure 4.

301

302   Surface AS4 is constrained as having formed between ~16-8 Ma (Hoke et al., 2007,

303   Evenstar et al., 2015). Within Quebrada Aroma (Fig. 1), the Nama ignimbrite is

304   interbedded with sediments that underlie surface AS4 placing an upper age

305   constraint of 16.27 ± 0.16 Ma on this surface (Pinto et al., 2004, Victor et al., 2004;

306   Farías et al., 2005; Pinto et al., 2007). Proximal to Quebrada Tana (Figs.1 and 4), the

307   Tana lava overlying this surface is dated at 8.8 ± 0.5 Ma (Mortimer et al., 1974 and

308   8.2 ± 0.5 Ma; Muñoz and Sepulveda, 1992) placing an upper age constraint on the

309   surface (Hoke et al., 2007). This surface is further constrained by *insitu* exposure

310   age dating to ~11 Ma (Fig. 4) (Evenstar et al., 2009, Evenstar et al., 2015 and

311   Evenstar et al., 2017).

312

313   Surface DS3 is constrained using *insitu* exposure age dating across the region to ~7

314   Ma (Kober et al., 2006, Evenstar et al., 2009, 2017). Several of the *insitu* exposure

315   ages lie on the landscape cross-profiles either on top of the residual palaeosurfaces

316   in the north or on the incised terrace surfaces in the south and are highlighted in

317   Figures 4 and 5C. Proximal to the Cerro Colorado mine DS3 links with the depth and

318   age of dated hematite within drill core at 7 Ma which records the paleowater table

319   level (Cooper et al., 2016) (Figure 4).

320

321   Surface DS2 was dated at ~3 Ma based on *insitu* exposure age dating (Fig. 4)

322   (Kober et al., 2006, Evenstar et al., 2009, 2017). The surface age can be further

323   constrained using the preservation of the Lluta ignimbrite (dated at 2.7 Ma; Wörner et

324   al., 2002) along fluvial terraces within Quebradas Lluta and Azapa (Fig. 4). Proximal

325   to the Cerro Colorado mine this surface is linked to dated hematite (3 Ma) within drill

326   core (Cooper et al., 2016) (Fig. 4).

327

328   **4.3 Reconstructing regional mean incision rates.**

329

330   The reconstructed fluvial paleo-surface profiles combined with the dating constraints

331   described above can be used to calculate the regional fluvial incision rates over the

332   last 11 million years (Fig. 6A). The difference in elevation between the paleo-fluvial

333 surfaces and modern river were extrapolated for each surface across the region (Fig.

334 6B). Using the difference in elevation of the surfaces and the modern river, divided by

335 the time since the surfaces had been abandoned the mean fluvial incision rates along

336 the main quebradas were calculated (Fig. 6C). In this way, we are able to reconstruct

337 relative incision rates for the PSS.

338

339 **5. Results**

340

341 Profile A runs 45 km from east to west at 18°45'S in Figure 3 and highlights the

342 general relationship of the surfaces within the region. AS4 is predominantly

343 preserved in the west of the Longitudinal Valley and shows an average depositional

344 slope of 5° to the west. Cutting into AS4 within the centre of the Longitudinal Valley,

345 DS3 incises 90 m and shows a similar depositional slope angle. To the east of DS3,

346 DS2 cuts 90 m into and erodes DS3, with a higher slope angle of 10° to the

347 west. Figure 4 highlights the overall relationship of the main fluvial archives from

348 North to South. AS4 forms the highest elevation surface across the region and is

349 predominantly preserved in the southern parts of the elevation profiles. DS3 cuts into

350 AS4 forming a lower elevation surface across the region. Cutting into both AS4 and

351 DS3, DS2 forms at the lowest elevation of all the preserved paleo-fluvial surface in

352 the Longitudinal Valley. The modern river system forms at the base of the valleys

353 with the lowermost elevations across the region. All the surfaces generally show an

354 increase in elevation towards the east and south across the region (Figure 3 and 4).

355 The changes in elevation show a step like increase from north to south and can be

356 separated into three different sectors (1 to 3 on Figure 4). Sector 1 runs from

357 (18°05'S) to Quebrada Tana (19°20'S), Sector 2 from Quebrada Tana (19°20'S) to

358 Quebrada Tarapaca (19°50'S) and Sector 3 from Quebrada Tarapaca (19°50'S) to

359 Quebrada Juan de Morales (20°10'S). Within each sector the change in elevation is

360 broadly similar and affects a number of different rivers rather than being river

361 specific. Sector 1 shows the highest changes in elevation across the region between

362 the different fluvial surfaces which decrease within Sector 2 and is the lowest within

363 Sector 3.

364

365 Figure 6A shows the current elevation of the fluvial systems in cross section B. AS4

366 shows a single laterally extensive surface which undulates across the region from

367 ~2750 masl in Sector 1, to ~2500 masl in Sector 2 and ~2650 masl in Sector 3. DS3

368 forms a laterally extensive surface with an average height of 2350 masl across

369 Sector 1 and 2 and increasing in elevation to ~2700 masl in Sector 3. DS2 varies in

370   elevation from 1800 masl at the northern tip of the elevation profile to ~ 2000 masl in

371   Sector 2 and increases in height to ~2600 masl in Sector 3. The modern fluvial

372   systems vary in height from 1400 masl to 1500 masl in Sector 1 to Sector 2 to ~2000

373   masl and ~2500 masl in Sector 3.

374

375   Using the difference between the paleo fluvial surfaces and modern fluvial systems

376   the change in fluvial incision through time can be more clearly illustrated (Fig. 6B).

377   and combined with the age constraint the fluvial incision rates through time can be

378   calculated (Fig. 6C). Overall, fluvial incision shows higher rates from 3 to present

379   day. However, there are marked differences across the study area. Sector 1 show

380   the highest rates of fluvial incision through time from 120 m/Myr at 11-7 Ma to 150

381   m/Myr at 7-3 Ma to ~200 m/Myr at 3-0 Ma. Sector 2 show lower incision rates

382   through time of 50 m/My for both 11-7 Ma and 7-3 Ma and higher rates of 100-50 for

383   3-0 Ma. Sector 3 show the lowest rates of fluvial incision throughout the area with 25

384   m/Myr from 11-7 Ma, 30m/Myr from 7-3 Ma and 50 m/Myr from 3-0 Ma.

385

386   **6. Discussion**

387

388   The geomorphic archive, using both pediplain and fluvial surfaces, is reconstructed

389   from Northernmost Chile and combined with age constraints to calculate fluvial

390   incision rates over a continental scale (>250 km) and back to the Miocene. These

391   data demonstrate three spatially marked changes in incision rates across the region,

392   from north to south. These distinctly different regions have been termed Sectors 1-3.

393   Sector 1 has the highest rates of fluvial incision through time (ca. 200 to 100 m/Myr),

394   Sector 2 show a lower rate of incision (ca. 100 to 50 m/Myr) and Sector 3 has the

395   lowest rates of incision (<50 m/Myr). These profiles show a generally continuous

396   drop in fluvial incision with slightly higher incision from 3 Ma to the present day. This

397   study shows that along the western margin of the Andes rates of fluvial incision can

398   vary dramatically over distances of 10's to 100's km. In Sector 1, incision rates of 100

399   m/m.y support those proposed by Hoke et al., (2007). However, in contrast to Hoke

400   et al., (2007) the incision shows a marked decrease to the south of Section 1 with

401   substantially lower rates in Section 2 and Section 3. These low rates correlate with

402   the incision rates documented in Cooper et al., (2016) explaining the disparity

403   between these two studies. Below we discuss what controls the variation in incision

404   rates in this region in order to evaluate their use as surface uplift makers.

405

406   The spatial extent of the area impacted (i.e. affecting multiple rivers per area

407   simultaneously) implies an external control. Such a control could take the form of (but
408   is not limited to) a change in relative terminal base level, climate or regional scale
409   tectonic uplift through fault blocks, rather than more localised internal river/catchment
410   specific causes (e.g. internal drainage reorganisation via river capture). Below we
411   discuss the major external controls on the compartmentalisation of the rivers within
412   this region.
413
414   **6.1 Uplift and fluvial incision**
415
416   **Regional tectonic uplift**
417   Fluvial incision rates have been used in numerous studies to help constrain uplift in
418   tectonically active areas (Maddy et al. 1997; Lave and Avouac 2001; Lu et al. 2004;
419   Whittaker et al., 2007). Although fluvial incision rates do not necessarily directly
420   translate to uplift rates as discharge may limit erosional capacity, they do give
421   minimum constraints. The sustained regional uplift of the Andean mountain chain is
422   broadly mirrored by continuous tectonically-driven fluvial incision throughout the
423   Miocene. However, this uplift is predominantly controlled by north-south fault
424   systems creating variation in uplift from West to East. There are no large scale east-
425   west trending structures which would generate marked changes in regional tectonic
426   uplift from North to South accounting for the compartmentalisation of the fluvial
427   incision rates.
428
429   **Terminal base level**
430   Comparison of Sector 1 and Sector 2 suggests a marked decrease in fluvial incision
431   through time and a marked change in terminal base level between the two fluvial
432   regions. In this part of the Andes the terminal base level is either external (sea level)
433   north of Quebrada Tana or internal (the Longitudinal valley, 1000 masl) south of
434   Quebrada Tana. Uniquely, Quebrada Tana acts as an endorheic drainage within the
435   Longitudinal Valley (Garcia et al., 2011; Kirk-Lawlor et al., 2013; Evenstar et al.,
436   2017). The timing of when fluvial systems north of Quebrada Tana became
437   exorheicly drained is diachronous from the Early to Mid Miocene *prior* to the fluvial
438   incision documented here (Evenstar et al., 2017). A change in base level would
439   initially lead to river profile adjustment affecting individual drainages, the absence of
440   observable river specific differences in the fluvial archives support the idea that in
441   Sector 1 rivers had an exorheic drainage prior to 11 Ma and so do not explain the
442   difference in fluvial incision rates between Sector 1 and Sector 2. However, the uplift
443   of the Coastal Cordillera has not been static during this time period. The uplift rate of

444 the Coastal Cordillera is poorly constrained, as discussed above. The base level of

445 the fluvial systems in the Longitudinal Valley terminate onto the eastern edge of the

446 Coastal Cordillera and are therefore affected by the regional scale uplift of the

447 mountain range rather than the uplift proximal to the coast which may be more

448 variable. The large scale and long term uplift of the mountain range varies from

449 between 50 m/Myr (0.05 mm/yr) to 70 m/Myr (0.07 mm/yr) (Delouis et al. 1998;

450 Hartley et al. 2000; Dunai et al. 2005; Cosentino and Jordan 2017). The difference

451 between the fluvial incision rate at Sector 1 compared to Sector 2, averaged over 11

452 Ma is 60m/Myr correlating with this value. Consequently, whilst Andean uplift to the

453 east generated significant fluvial incision within the Longitudinal Valley this was

454 partially offset in Sector 2 and 3 (the endorheicly-drained region) by simultaneous

455 uplift of the Coastal Cordillera in the west. In essence, the rate of fluvial incision is

456 controlled by the east to west length of the fluvial system and whether rivers cut the

457 uplifting north-south trending Coastal Cordillera. The difference between the reach of

458 Sector 1 and Sector 2 is highlighted in Figure 1B.

459

460 **Tectonic beheading**

461

462 The change in fluvial incision rates from Sector 2 to 3 are more challenging to

463 explain. Both sectors have the same terminal base level within the Longitudinal

464 Valley of ~1000 masl. However, there is a sharp change in the catchment length of

465 major fluvial systems entering the Longitudinal Valley from between the two regions

466 (Fig. 7). Throughout the region, 18°20''S to 22°00' S, the fluvial systems have been

467 constrained by Hoke et al., 2007 as ranging in drainage area from 5 x 10^9 km^2 to 9 x

468 10^8 km^2 and in length from 30 to 170 km, with both values decreasing towards the

469 south (Fig. 7). Significantly, these data demonstrate a sudden decrease in fluvial

470 lengths from 110 km to 80 km between Sector 2 and Sector 3 (Figs.1 and 7). This

471 length-gap coincides with a sudden shift in the edge of the watershed from along the

472 western edge of the Western Cordillera to along the Cordillera de Domeyko fault

473 system in the central Precordillera suggesting a tectonically configured watershed.

474 The uplift along the Cordillera de Domeyko fault system beheads the upper part of

475 the drainages within Sector 3, reducing their length by approx. 30 km (Figs. 1 and 7).

476 The affected fluvial systems in this region thus only record the minimum uplift over

477 the Longitudinal Valley and Precordillera as they are no longer connected to the

478 highest elevation areas of the mountain range further east (Fig. 1B). The difference

479 in fluvial incision rates between Sector 2 and Sector 3 of 25 m/Myr to 50 m/Myr

480 therefore place constraints on the uplift generated between the central and eastern

481 edge of the Precordillera.

482

483 **6.2 Alternative controls on fluvial incision**

484

485 Whilst the observed spatial differences in fluvial incision rates over the region can be

486 largely explained by tectonic controls it is important to briefly explore alternative

487 explanations for these regional differences within the study area that can operate on

488 a similar spatial scale, principally climate and bedrock. It has been suggested that the

489 present-day rivers within the study area vary in erosional capacity from north to south

490 as a function of mean annual precipitation within the source regions (Garcia et al

491 2011). Quebrada Lluta has a catchment with a present-day mean annual

492 precipitation rate of 200 mm/yr, Quebradas Azapa, Victor and Camarones have rates

493 of 100 mm/yr and south of Quebrada Camarones the river catchments have rates of

494 < 100 mm/yr (Garcia et al., 2011). However, it is unlikely that latitudinal variations in

495 rainfall are the main cause for incision patterns observed across the region as there

496 is no apparent spatial link between the precipitation rates and the change in fluvial

497 incision rates. For example, there is no change in the fluvial incision between

498 Quebrada Lluta and the rivers to the south, despite Quebrada Lluta draining an area

499 with much higher mean annual precipitation. If precipitation rates do place some

500 control on incision rates it must be at a much smaller scale than the tectonic controls.

501

502 Fluvial research demonstrates that the strength properties of bedrock lithology can

503 impact on fluvial system incisional behaviour (e.g. Stokes et al., 2017) and could thus

504 potentially account for spatial variations in incision rates across the study area.

505 However, whilst there is a difference *between* the major N-S morphotectonic units

506 (thereby presenting an E-W variability in potential erodibility across the region), there

507 is little N-S variation *within* these units that can account for the observed N-S

508 spatially compartmentalised incision rates.

509

510 **6.3 Controls on fluvial incision in Northern Chile**

511

512 Fluvial incision rates have been used in numerous studies to help constrain uplift in

513 tectonically active areas (Lave and Avouac 2001; Lu et al. 2004; Whittaker et al.,

514 2007; Anton et al., 2014; Stokes et al. 2018). The fluvial regions along the edge of

515 the Andes have varying east-west extent over the north-south orientated tectonic

516 provinces. The fluvial incision therefore shows marked compartmentalization across

517 the region with a step like increase from south to north. The varying reaches of the

518 rivers and the differences in fluvial incision rates between these reaches can
519 therefore be exploited to place minimum constraints on the different tectonic
520 provinces through time.
521
522 Sector 1, which spans from the Pacific Ocean to the western edge of the Western
523 Cordillera (Figure 1B), constrains the uplift on a continental-scale along the edge of
524 the Andes. This constrains the uplift of this region (the western side of the Andes) to
525 a minimum of 1200m in 11 Myr. This supports previous models of Late Miocene uplift
526 (e.g. Garzione et al., 2006; Ghosh et al., 2006, Garzione et al., 2008) however in
527 contrast to these models it suggests uplift continued at a slower rate from 7 to 3 Ma
528 and at a higher rates from 3 to 0 Ma (120 m/Myr at 11-7 Ma to 150 m/Myr at 7-3 Ma
529 to ~200 m/Myr at 3-0 Ma).
530
531 Sector 2 spans from the Longitudinal Valley to the western edge of the Western
532 Cordillera (Fig. 1B) constraining the uplift over the western margin of the Andes
533 minus uplift of the Coastal Cordillera. Therefore, the difference between Sector 1 and
534 Sector 2 of 60 m/Myr records the uplift of the Coastal Cordillera which corresponds
535 with published uplift rates for the Coastal Cordillera of between 50 m/Myr (0.05
536 mm/yr) to 70 m/Myr (0.07 mm/yr) (Delouis et al. 1998; Hartley et al. 2000; Dunai et
537 al. 2005).
538
539 Sector 3, spans a much shorter extent than Sectors 1 and 2, from the Longitudinal
540 Valley to the Cordillera de Domeyko fault system in the central Precordillera (Fig.
541 1B). The difference between Sectors 2 and 3, of 25 m/Myr to 50 m/Myr, therefore
542 places a minimum constraint on the uplift generated between the central and eastern
543 edge of the Precordillera along the Cordillera de Domeyko fault system.
544
545 **7. Conclusions**
546
547 Within the Atacama Desert, Northern Chile, slow long-term erosion creates
548 exceptional preservation of geomorphic archives (fluvial and pediment surfaces)
549 allowing the long-term reconstruction of fluvial archives on a continental scale. In this
550 study, fluvial profiles are constructed over a wide region (>250 km) along the western
551 margin of the Andes (18°00'S to 20°15'S) and over a time frame from Miocene to
552 Present day. The results reveal that incision patterns reconstructed over a wide area
553 running perpendicular to the main fluvial systems allows a greater spatial and
554 temporal understanding of uplift, specifically;

555

- Fluvial incision can be reconstructed for ~11 Ma, ~7 Ma, ~3 Ma and the modern day.
- Fluvial incision shows marked spatial compartmentalization across the region with a step like increase from south to north.
- Sector 1 has the highest rates of fluvial incision through time (ca. 200 to 100 m/Myr), Sector 2 shows a lower rate of incision (ca. 100 to 50 m/Myr) and Sector 3 has the lowest rates of incision (<50 m/Myr).
- The main control on the rate of fluvial incision is the extent of the east to west reach of the main rivers across the north to south tectonic provinces.
- Sector 1 spans the entire Coastal Cordillera, Longitudinal Valley and Precordillera to the western edge of the Western Cordillera. This constrains uplift of this region (the western side of the Andes) to a minimum of 1200m in 11 Myr which supports Late Miocene uplift however contrary to these models, it suggests uplift continued at a higher rate from 3 to the present day.
- Sector 2 only spans the Longitudinal Valley and the Precordillera to the western edge of the Western Cordillera. The absence of fluvial systems cutting the Coastal Cordillera accounts for the reduced incision rates of 60 m/Myr which correspond to the published uplift rates for the Coastal Cordillera of 60 m/Myr.
- The eastern edge of Sector 3 is constrained by the Cordillera Domeyko fault system within the Central Precordillera. As such, Sector 3 only places constraints on uplift of the Longitudinal Valley and the western edge of the Precorillera. The absence of the eastern edge of the Precordillera accounts for the decrease in incision rates within this area and places a constraint of uplift generated here in the region of 25 m/Myr to 50 m/Myr.

581

Most Quaternary fluvial studies tend to be restricted to detailed examination of a single river to understand long-term uplift or climate, mainly due to the scale and intensity of research required to unravel the incision history. Whilst this provides a wealth of knowledge regarding uplift over the reach of the fluvial system, in order to understand orographic scale uplift (and rule out river specific controls) a more regional overview of the fluvial base-level changes is required. Such studies have the potential to address not just the timing of uplift on a continental scale but also any regional spatial controls such as the relative uplift of individual tectonic provinces.

590

9. References

Antón, L., De Vicente, G., Muñoz-Martín, A., & Stokes, M. (2014). Using river long profiles and geomorphic indices to evaluate the geomorphological signature of continental scale drainage capture, Duero basin (NW Iberia). Geomorphology, 206, 250-261.

Barnes, J. B., & Ehlers, T. A. (2009). End member models for Andean Plateau uplift. Earth-Science Reviews, 97(1-4), 105-132.

Benito, G., Gutiérrez, F., Pérez-González, A., & Machado, M. J. (2000). Geomorphological and sedimentological features in Quaternary fluvial systems affected by solution-induced subsidence (Ebro Basin, NE-Spain). Geomorphology, 33(3-4), 209-224.

Boulton, S. J., Stokes, M., & Mather, A. E. (2014). Transient fluvial incision as an indicator of active faulting and Plio-Quaternary uplift of the Moroccan High Atlas. Tectonophysics, 633, 16-33.

Bridgland, D. R., Westaway, R., Romieh, M. A., Candy, I., Daoud, M., Demir, T. & Shaw, A. D. (2012). The River Orontes in Syria and Turkey: Downstream variation of fluvial archives in different crustal blocks. Geomorphology, 165, 25-49.

Cooper, F., Adams, B., Blundy, J., Farley, K., McKeon, R., & Ruggiero, A. (2016). Aridity-induced Miocene canyon incision in the Central Andes. Geology, 44(8), 675-678.

Cosentino, N. J., Jordan, T. E., Derry, L. A., & Morgan, J. P. (2015). 87Sr/86Sr in recent accumulations of calcium sulfate on landscapes of hyperarid settings: A bimodal altitudinal dependence for northern C hile (19.5° S–21.5° S). Geochemistry, Geophysics, Geosystems, 16(12), 4311-4328.

628

629

630 Cyr, A. J., Granger, D. E., Olivetti, V., & Molin, P. (2010). Quantifying rock uplift rates
631 using channel steepness and cosmogenic nuclide–determined erosion rates:
632 Examples from northern and southern Italy. Lithosphere, 2(3), 188-198.

633

634 Delouis, B., Philip, H., Dorbath, L., & Cisternas, A. (1998). Recent crustal
635 deformation in the Antofagasta region (northern Chile) and the subduction process.
636 Geophysical Journal International, 132(2), 302-338.

637

638 Demoulin, A., Bovy, B., Rixhon, G., & Cornet, Y. (2007). An automated method to
639 extract fluvial terraces from digital elevation models: The Vesdre valley, a case study
640 in eastern Belgium. Geomorphology, 91(1-2), 51-64.

641

642 Demoulin, A., Mather, A., & Whittaker, A. (2017). Fluvial archives, a valuable record
643 of vertical crustal deformation. Quaternary Science Reviews, 166, 10-37.

644

645 Dunai, T. J., Gonzalez-Lopez, G. A., Juez-Larre, J., & Carrizo, D. (2005).
646 Preservation of (early) miocence landscapes in the Atacama Desert, northern Chile.
647 Geochimica Et Cosmochimica Acta, 69(10), A161-A161.

648

649 Ehlers, T. A., & Poulsen, C. J. (2009). Influence of Andean uplift on climate and
650 paleoaltimetry estimates. Earth and Planetary Science Letters, 281(3-4), 238-248.

651

652 Evenstar, L., Mather, A., Hartley, A., Stuart, F., Sparks, R., & Cooper, F. (2017).
653 Geomorphology on geologic timescales: Evolution of the late Cenozoic Pacific
654 paleosurface in Northern Chile and Southern Peru. Earth-Science Reviews. 71, 1-27.

655

656 Evenstar, L. A., Hartley, A. J., Stuart, F. M., Mather, A. E., Rice, C. M., & Chong, G.
657 (2009). Multiphase development of the Atacama Planation Surface recorded by
658 cosmogenic He-3 exposure ages: Implications for uplift and Cenozoic climate change
659 in western South America. Geology, 37(7), 658-658.

660

661 Evenstar, L. A., Stuart, F. M., Hartley, A. J., & Tattitch, B. (2015). Slow Cenozoic
662 uplift of the western Andean Cordillera indicated by cosmogenic 3He in alluvial
663 boulders from the Pacific Planation Surface. Geophysical Research Letters, 42(20),
664 8448-8455.

665

666 Evenstar, L. A., Sparks, R. S. J., Cooper, F. J., & Lawton, M. N. (2018). Quaternary

667 landscape evolution of the Helmand Basin, Afghanistan: Insights from staircase

668 terraces, deltas, and paleoshorelines using high-resolution remote sensing

669 analysis. Geomorphology, 311, 37-50.

670

671 Farías, M., Charrier, R., Comte, D., Martinod, J., & Hérail, G. (2005). Late Cenozoic

672 deformation and uplift of the western flank of the Altiplano: Evidence from the

673 depositional, tectonic, and geomorphologic evolution and shallow seismic activity

674 (northern Chile at 19°30′S). Tectonics, 24(4), TC4001.

675

676 Garcia, M., & Herail, G. (2005). Fault-related folding, drainage network evolution and

677 valley incision during the Neogene in the Andean Precordillera of Northern Chile.

678 Geomorphology, 65(3-4), 279-300.

679

680 Garcia, M., Riquelme, R., Farías, M., Herail, G., & Charrier, R. (2011). Late Miocene-

681 Holocene canyon incision in the western Altiplano, northern Chile: tectonic or climatic

682 forcing? Journal of the Geological Society, 168(4), 1047-1060.

683

684 García-Pérez, T., Marquardt, C., Yáñez, G., Cembrano, J., Gomila, R., Santibañez,

685 I., & Maringue, J. (2018). Insights on the structural control of a Neogene forearc

686 basin in Northern Chile: A geophysical approach. Tectonophysics, 736, 1-14.

687

688 Garzione, C. N., Hoke, G. D., Libarkin, J. C., Withers, S., MacFadden, B., Eiler, J. &

689 Mulch, A. (2008). Rise of the Andes. Science, 320(5881), 1304-1307.

690

691 Garzione, C. N., Molnar, P., Libarkin, J. C., & MacFadden, B. J. (2006). Rapid late

692 Miocene rise of the Bolivian Altiplano: Evidence for removal of mantle lithosphere.

693 Earth and Planetary Science Letters, 241(3-4), 543-556.

694

695 Gesch, D. B. (2014). An inventory of topographic surface changes; the value of

696 multitemporal elevation data for change analysis and monitoring. ISPRS Annals of

697 Photogrammetry, Remote Sensing & Spatial Information Sciences, 2(4).

698

699 Ghosh, P., Garzione, C. N., & Eiler, J. M. (2006). Rapid uplift of the Altiplano

700 revealed through C-13-O-18 bonds in paleosol carbonates. Science, 311(5760), 511-

701 515.

702

703 Hartley, A. J., Chong, G., Houston, J., & Mather, A. E. (2005). 150 million years of

704 climatic stability: evidence from the Atacama Desert, northern Chile. Journal of the

705 Geological Society, 162(3), 421-424.

706

707 Hartley, A. J., & Evenstar, L. (2010). Cenozoic stratigraphic development in the north

708 Chilean forearc: Implications for basin development and uplift history of the Central

709 Andean margin. Tectonophysics, 495(1-2), 67-77.

710

711 Hartley, A. J., May, G., Chong, G., Turner, P., Kape, S. J., & Jolley, E. J. (2000).

712 Development of a continental forearc: A Cenozoic example from the Central Andes,

713 northern Chile. Geology, 28(4), 331-334.

714

715 Hartley, A. J., Sempere, T., & Wörner, G. (2007). A comment on "Rapid late Miocene

716 rise of the Bolivian Altiplano: Evidence for removal of mantle lithosphere" by C.N.

717 Garzione et al. [Earth Planet. Sci. Lett. 241 (2006) 543-556]. Earth and Planetary

718 Science Letters, 259(3-4), 625-629.

719

720 Hoke, G. D., Isacks, B. L., Jordan, T. E., Blanco, N., Tomlinson, A. J., & Ramezani, J.

721 (2007). Geomorphic evidence for post-10 Ma uplift of the western flank of the central

722 Andes 18°30′-22°S. Tectonics, 26(5), TC5021

723

724

725 Hu, X., Pan, B., Kirby, E., Li, Q., Geng, H., & Chen, J. (2010). Spatial differences in

726 rock uplift rates inferred from channel steepness indices along the northern flank of

727 the Qilian Mountain, northeast Tibetan Plateau. Chinese Science Bulletin, 55(27-28),

728 3205-3214.

729

730 Jordan, T. E., Kirk-Lawlor, N. E., Blanco P., N., Rech, J. A., & Cosentino, N. J.

731 (2014). Landscape modification in response to repeated onset of hyperarid

732 paleoclimate states since 14 Ma, Atacama Desert, Chile. Geological Society of

733 America Bulletin. 126(7/7), 1016-1046

734

735 Juez-Larré, J., Kukowski, N., Dunai, T. J., Hartley, A. J., & Andriessen, P. A. (2010).

736 Thermal and exhumation history of the Coastal Cordillera arc of northern Chile

737 revealed by thermochronological dating. Tectonophysics, 495(1), 48-66.

738

739   Kirk-Lawlor, N. E., Jordan, T. E., Rech, J. A., & Lehmann, S. B. (2013). Late Miocene
740   to Early Pliocene paleohydrology and landscape evolution of Northern Chile, 19 to 20
741   S. Palaeogeography, Palaeoclimatology, Palaeoecology, 387, 76-90.
742
743   Kober, F., Ivy-Ochs, S., Schlunegger, F., Baur, H., Kubik, P. W., & Wieler, R. (2007).
744   Denudation rates and a topography-driven rainfall threshold in northern Chile:
745   Multiple cosmogenic nuclide data and sediment yield budgets. Geomorphology, 83(1-
746   2), 97-120.
747
748   Kober, F., Schlunegger, F., Zeilinger, G., & Schneider, H. (2006). Surface uplift and
749   climate change: The geomorphic evolution of the Western Escarpment of the Andes
750   of northern Chile between the Miocene and present. Tectonics, Climate, and
751   Landscape Evolution, 398, 75-86.
752
753   Lavé, J., & Avouac, J.-P. (2000). Active folding of fluvial terraces across the Siwaliks
754   Hills, Himalayas of central Nepal. Journal of Geophysical Research: Solid Earth,
755   105(B3), 5735-5770.
756
757   Litchfield, N., & Berryman, K. (2006). Relations between postglacial fluvial incision
758   rates and uplift rates in the North Island, New Zealand. Journal of Geophysical
759   Research: Earth Surface, 111(F2).
760
761   Lu, H., Wang, X., An, Z., Miao, X. D., Zhu, R. X., Ma, H. Z., & Wang, X. Y. (2004).
762   Geomorphologic evidence of phased uplift of the north eastern Qinghai-Tibet Plateau
763   since 14 million years ago. Science in the China Series D Earth Science-English
764   edition, *47*, 822-833.
765
766   Macklin, M. G., Fuller, I. C., Lewin, J., Maas, G. S., Passmore, D. G., Rose, J., &
767   Rowan, J. S. (2002). Correlation of fluvial sequences in the Mediterranean basin over
768   the last 200 ka and their relationship to climate change. Quaternary Science
769   Reviews, 21(14-15), 1633-1641
770
771   Maddy, D. (1997). Uplift-driven valley incision and river terrace formation in southern
772   England. Journal of Quaternary Science: Published for the Quaternary Research
773   Association, 12(6), 539-545.
774
775   Madella, A., Delunel, R., Audin, L., & Schlunegger, F. (2016). Why is there no

776   Coastal Cordillera at the Arica Bend (Western Central Andes)? Basin Research.

777   Mortimer C., F. E. a. S. N. (1974). K-Ar ages from tertiary lavas of the northernmost

778   Chilean Andes. Geologische Rundschau, 63, 484 - 493.

779

780   Martins, A. A., Cabral, J., Cunha, P. P., Stokes, M., Borges, J., Caldeira, B., &

781   Martins, A. C. (2017). Tectonic and lithological controls on fluvial landscape

782   development in central-eastern Portugal: Insights from long profile tributary stream

783   analyses. Geomorphology, 276, 144-163.

784

785   Montgomery, D. R., & Brandon, M. T. (2002). Topographic controls on erosion rates

786   in tectonically active mountain ranges. Earth and Planetary Science Letters, *201*(3-

787   4), 481-489.

788

789   Muñoz, N., Sepúlveda, p. (1992). Estructuras compressivas con vergencia al Oeste

790   en el borde oriental de la Depresión Central (19°15' lat. Sur). Revista Geologica De

791   Chile, 19, 214-247.

792

793   Noble, D. C., Sébrier, M., Megard, F., & McKee, E. H. (1985). Demonstration of two

794   pulses of Paleogene deformation in the Andes of Peru. Earth and Planetary Science

795   Letters, 73(2), 345-349.

796

797   Pinto, L., Hérail, G., Charrier, R. (2004). Syntectonic sedimentation associated with

798   Neogene structures in the Precordillera of Moquella Zone, Tarapacá (19°15'S,

799   northern Chile). Revista Geologica De Chile, 31, 19-44.

800

801   Pinto, L., Hérail, G., Fontan, F., & de Parseval, P. (2007). Neogene erosion and uplift

802   of the western edge of the Andean Plateau as determined by detrital heavy mineral

803   analysis. Sedimentary Geology, 195(3-4), 217-237.

804

805   Rech, J. A., Currie, B. S., Jordan, T. E., Riquelme, R., Lehmann, S. B., Kirk-Lawlor,

806   N. E., & Gooley, J. T. (2019). Massive middle Miocene gypsic paleosols in the

807   Atacama Desert and the formation of the Central Andean rain-shadow. Earth and

808   Planetary Science Letters, 506, 184-194.

809

810   Regard, V., Saillard, M., Martinod, J., Audin, L., Carretier, S., Pedoja, K., ... & Hérail,

811   G. (2010). Renewed uplift of the Central Andes Forearc revealed by coastal evolution

812   during the Quaternary. Earth and Planetary Science Letters, 297(1-2), 199-210.

813

814 Schildgen, T., Dethier, D. P., Bierman, P., & Caffee, M. (2002). ^{26}Al and ^{10}Be dating

815 of late Pleistocene and Holocene fill terraces: a record of fluvial deposition and

816 incision, Colorado Front Range. Earth Surface Processes and Landforms, 27(7),

817 773-787.

818

819 Schildgen, T. F., Ehlers, T. A., Whipp, D. M., van Soest, M. C., Whipple, K. X., &

820 Hodges, K. V. (2009). Quantifying canyon incision and Andean Plateau surface uplift,

821 southwest Peru: A thermochronometer and numerical modeling approach. Journal of

822 Geophysical Research, 114(F4).

823

824 Stokes, M., Mather, A., Belfoul, M., Faik, F., Bouzid, S., Geach, M., & Thiel, C.

825 (2017). Controls on dryland mountain landscape development along the NW Saharan

826 desert margin: Insights from Quaternary river terrace sequences (Dadès River,

827 south-central High Atlas, Morocco). Quaternary Science Reviews, 166, 363-379.

828

829 Stokes, M., Mather, A., Rodés, Á., Kearsey, S., & Lewin, S. (2018). Anatomy, age

830 and origin of an intramontane top basin surface (Sorbas Basin, Betic Cordillera, SE

831 Spain). Quaternary, 1(2), 15

832

833 Thouret, J.-C., Wörner, G., Gunnell, Y., Singer, B., Zhang, X., & Souriot, T. (2007).

834 Geochronologic and stratigraphic constraints on canyon incision and Miocene uplift

835 of the Central Andes in Peru. Earth and Planetary Science Letters, 263(3), 151-166.

836

837 van Zalinge, M. E., Sparks, R. S. J., Evenstar, L. A., Cooper, F. J., Aslin, J., &

838 Condon, D. J. (2017). Using ignimbrites to quantify structural relief growth and

839 understand deformation processes: Implications for the development of the Western

840 Andean Slope, northernmost Chile. Lithosphere, 9(1), 29-45.

841

842 Victor, P., Oncken, O., & Glodny, J. (2004). Uplift of the western Altiplano plateau:

843 Evidence from the Precordillera between 20° and 21°S (northern Chile). Tectonics,

844 23(4), TC4004.

845

846 Wörner, G., Hammerschmidt, K., Henjes-Kunst, F., Lezaun, J., & Wilke, H. (2000).

847 Geochronology (40Ar/39Ar, K-Ar and He-exposure ages) of Cenozoic magmatic

848 rocks from northern Chile (18-22 S): implications for magmatism and tectonic

849 evolution of the central Andes. Revista geológica de Chile, 27(2), 205-240.

850

851   Whittaker, A. C., Cowie, P. A., Attal, M., Tucker, G. E., & Roberts, G. P. (2007).

852   Bedrock channel adjustment to tectonic forcing: Implications for predicting river

853   incision rates. Geology, 35(2), 103-106.

854

855   Wörner, G., Uhlig, D., Kohler, I., & Seyfried, H. (2002). Evolution of the West Andean

856   Escarpment at 18°S (N. Chile) during the last 25 Ma: uplift, erosion and collapse

857   through time. Tectonophysics, 345(1–4), 183-198.

858

859   Wotzlaw, J. F., Decou, A., von Eynatten, H., Wörner, G., & Frei, D. (2011). Jurassic

860   to Palaeogene tectono-magmatic evolution of northern Chile and adjacent Bolivia

861   from detrital zircon U-Pb geochronology and heavy mineral provenance. Terra Nova,

862   23(6), 399-406.

863

864   **10. Figures**

A

30 km

N

18°S

Peru

70°W

69°

Bolivia

A'

Pacific Ocean

Q. Lluta
Q. Azapa

Q.Victor

A

19°S

Q. Camarones

Q. Tana

Q. A

Tectonics

Coastal Cordillera

Longitudinal Valley

Precordillera

Major Faults

Fluvial Systems

Main Rivers

Catchment area

Q. T

Q. Q

Iquique

Q. JdM

B

Sector 1

Sector 2

Sector 3

A

A'

4
3
2
1

km

Coastal Cordillera | Longitudinal Valley | Precordillera | Western Cordillera

865
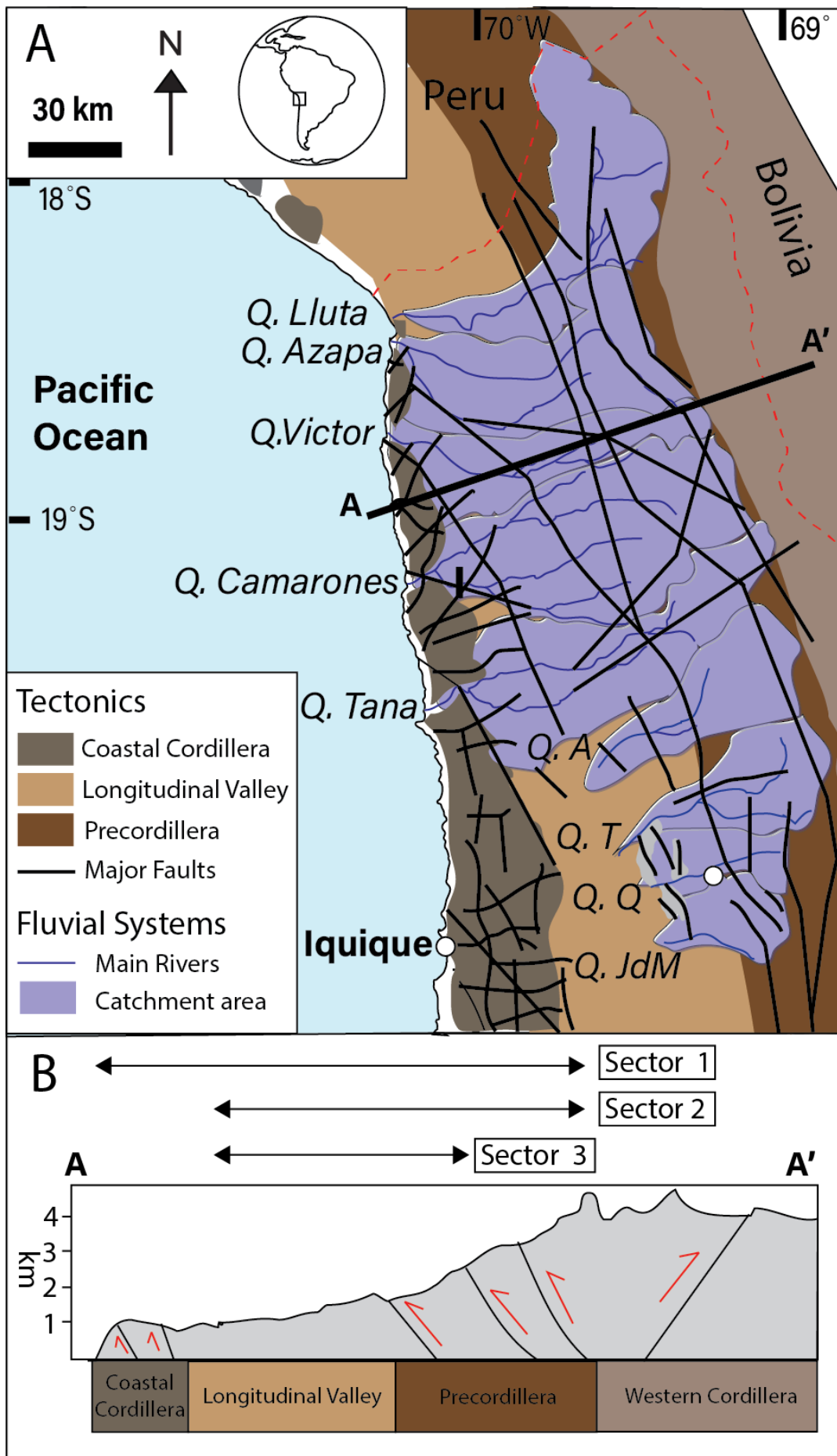
866   **Figure 1;** a) Sketch of Central Andes showing the five morphotectonic provinces.
867   The main sectors and the fluvial systems within them are highlighted showing
868   catchment area (b) Cross section of main morphotectonic provinces, location shown
869   in Figure 1A. Major tectonics features of the region (Garcia et al., 2004; Victor et al.,
870   2004; Farías et al., 2005; Juez-Larre et al., 2010; Allmendinger and Gonzalez 2014;).
871   Length of reach of the major Sectors (1-3) over the morphotectonic provinces are
872   highlighted.
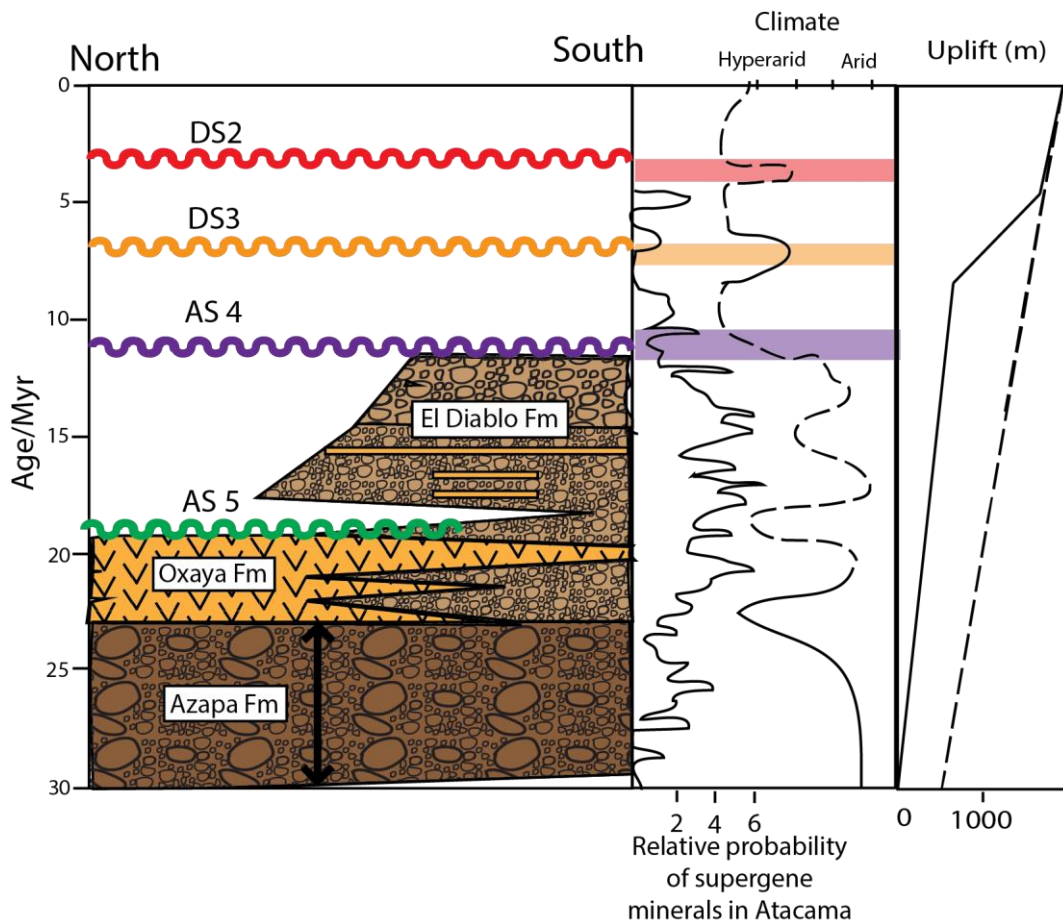
873

874   **Figure 2;** (from left to right) Basic sedimentary overview of the Longitudinal Valley in
875   the study area with the main geomorphic surfaces (AS5, AS4, DS3 and DS2).
876   Climate profile for Longitudinal Valley (Jordan et al. 2014 and Evenstar et al. 2017)
877   with timing for main geomorphic surfaces highlighted and timing of supergene
878   minerals in Atacama (Aranciabia et al. 2009). Elevation profiles for Longitudinal
879   Valley from Evenstar et al. 2015. Solid line represents Late Miocene uplift and
880   dashed line Early Miocene uplift.

881
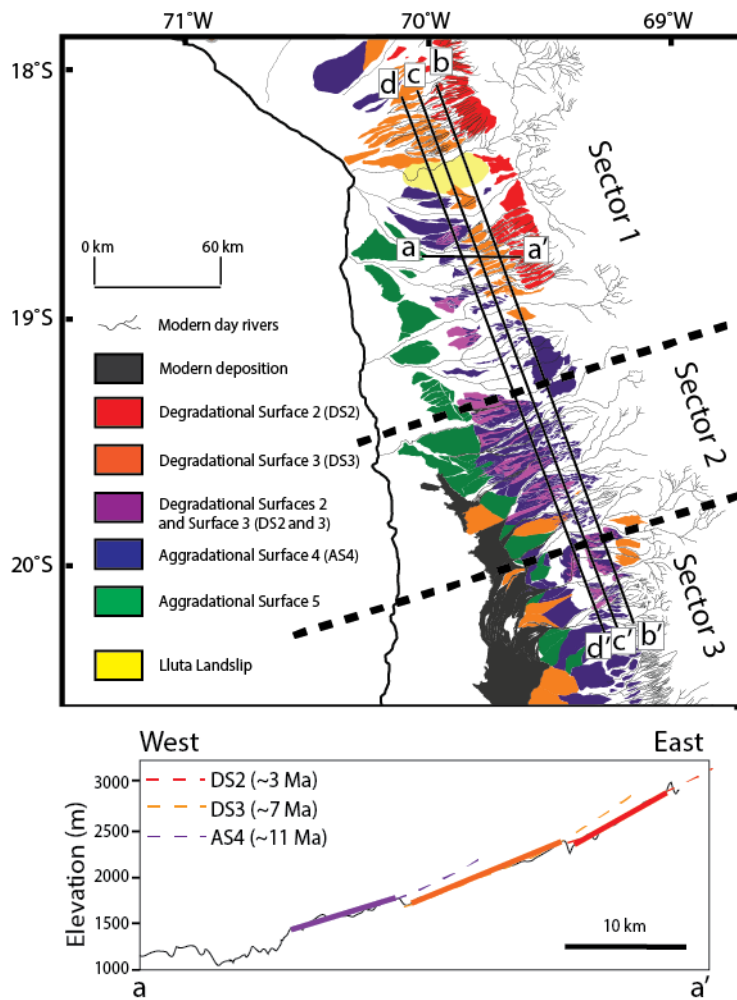
Figure 3. (Upper) Large scale map of Northern Chile showing the geomorphic surfaces (1-5) that form the Pacific Paleosurface (PPS). Black lines highlight the topographic cross sections (a-d) in figures 5. Black dashed lines separate regions of Sector 1-3. (Lower) Profile A shows a profile taken west to east across the Longitudinal Valley showing increasing incision of the paleosurfaces to the east through time.
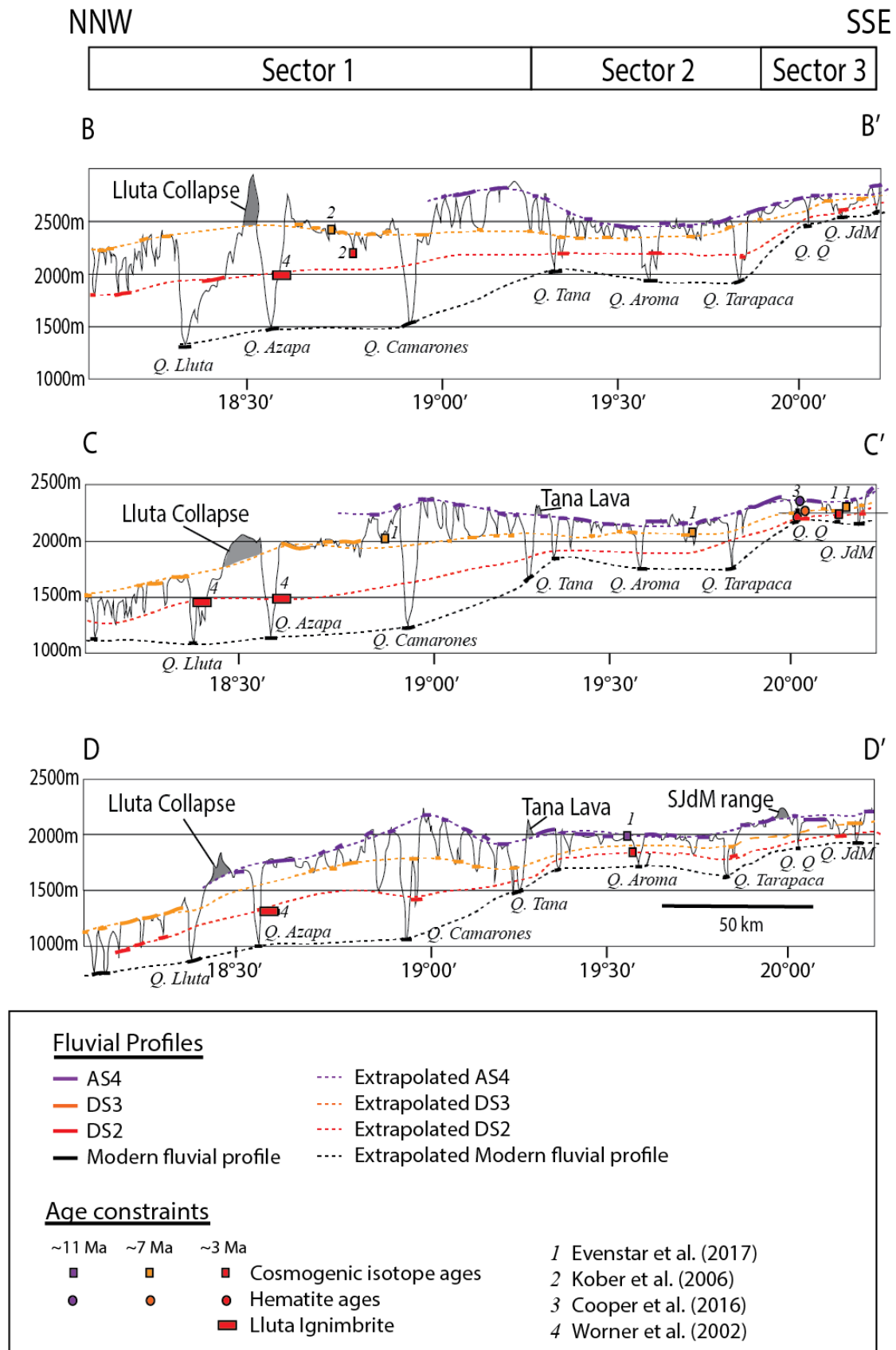
**Figure 4;** Three cross sections across the region. Locations shown in figure 3.
Profiles b-d are taken NNW to SSE. Black lines shows the topographic cross
sections across the region. Solid colour lines show the preserved parts of the surface

892   with the coloured dashed lines highlight the reconstructed paleo fluvial profiles

893   associated with each surface (AS 4, DS3, DS2 and the modern). Grey areas

894   represent anomalies on the topography profile. Key shows the main features that

895   control the age of the surfaces.
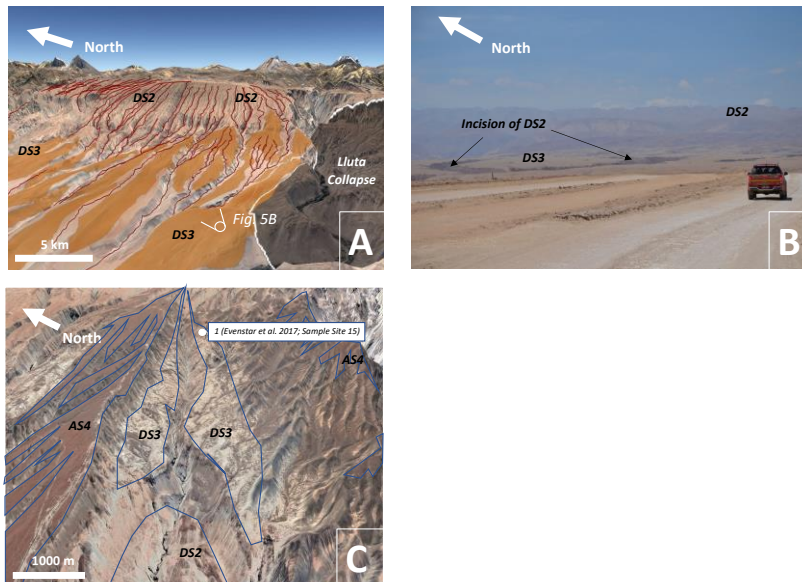
896

897   **Figure 5;** A) Google Earth image with 3x vertical exaggeration of DS2 cutting into

898   DS3, leaving DS3 as a series of relict inselberg highs north of Quebrada Lluta.

899   Location of photo of Figure 5B shown, B) Photo of same view taken from the field

900   showing incision of DS3 by DS2 C) Google Earth image with 3x vertical exaggeration

901   of DS3 and DS2 cutting into AS4 forming a lower terrace in Quebrada Camarones

902   with site location of *insitu* exposure age dating in Evenstar et al. 2017.
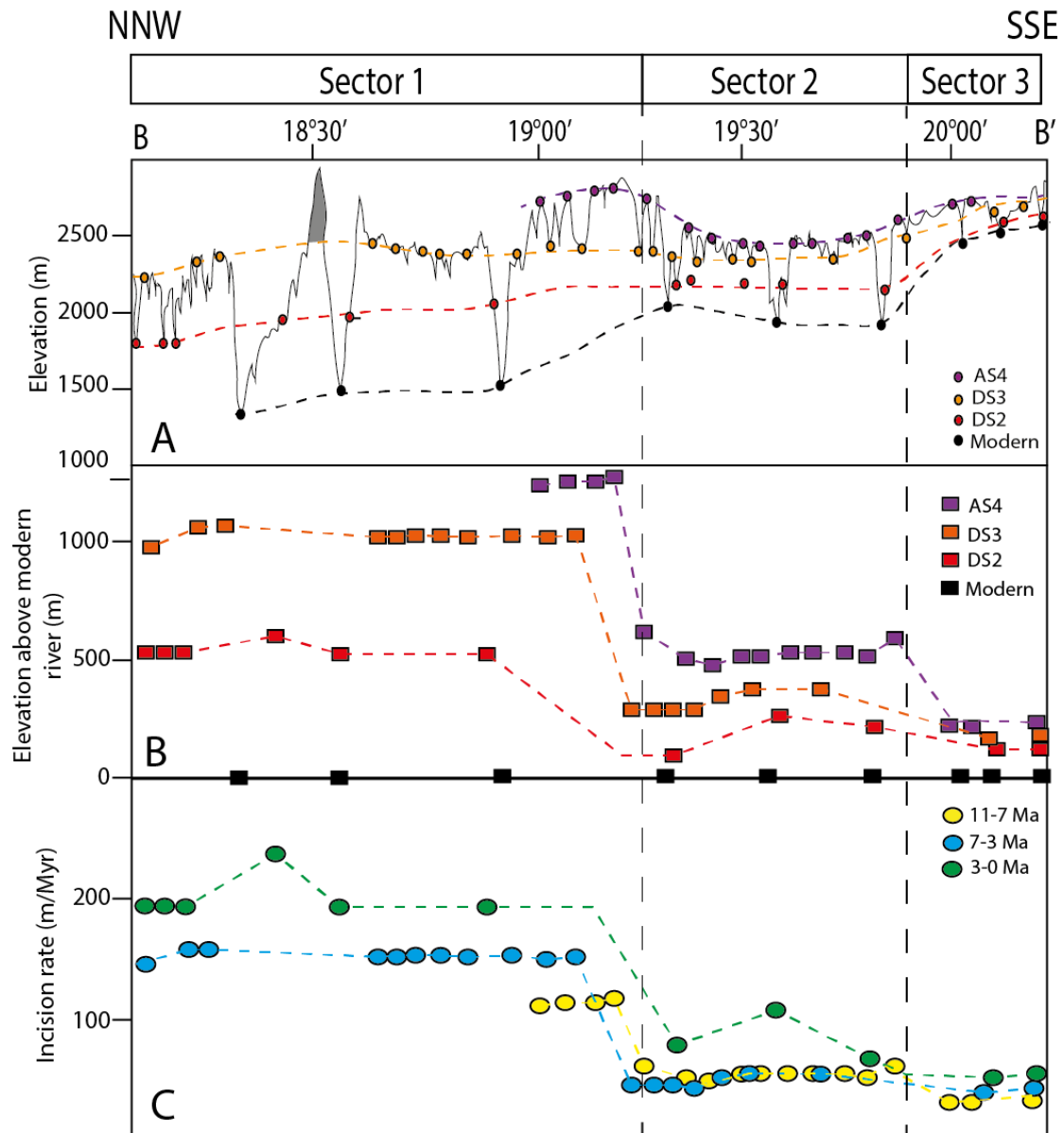
903
904 **Figure 6; A-** Cross section B showing the different paleo fluvial surfaces draped over
905 an elevation profile. Coloured dots represent locations where the elevation was takes
906 for Figure 6 B-C. **B** Shows the difference between paleo fluvial surfaces and modern
907 fluvial profiles. **C** Incision rate through time calculated using the difference in
908 elevation between the paleo fluvial surfaces and modern fluvial system divided by
909 age of paleo fluvial surface.

910
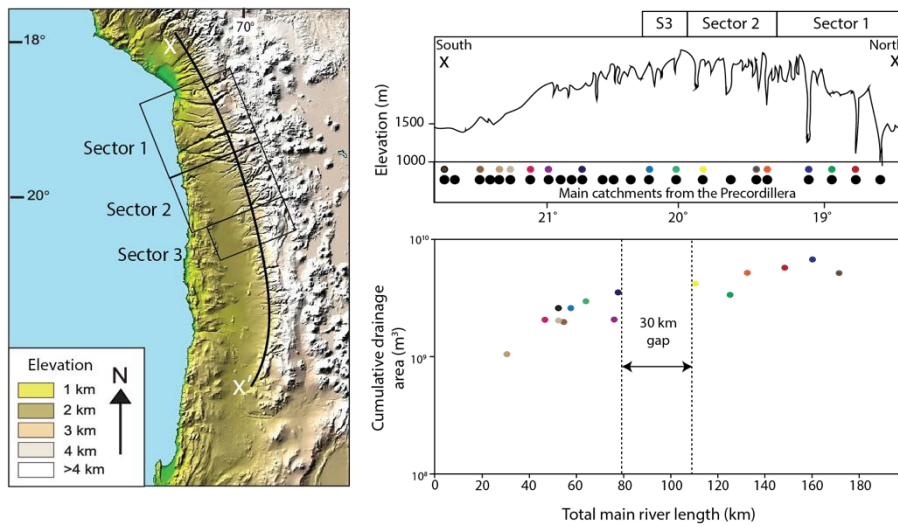
Figure 7; (Top) Elevation profile along the eastern edge of the Longitudinal Valley
from Evenstar et al., 2017 highlighting study area (Sector 1, Sector 2 and Sector 3
(S3)). At the base of the elevation profile the black dots show the main fluvial
systems from the Precordillera (the coloured dots relate to the dots in the cumulative
drainage area graph below). (Bottom) cumulative drainage area of studied fluvial
systems against length of fluvial system, this data was initially presented in Hoke et
al. 2007 (supplementary material). a summary of cumulative drainage areas and
fluvial length (distance from mouth) (Supplementary material in Hoke et al. 2007
which have been combined and summarized in this paper)